CHAPTER 22

Films for Electrochemical Applications

MACARENA J. MONTENEGRO and THOMAS LIPPERT

Paul Scherrer Institut, General Energy Research Department, Villigen, Switzerland

22.1 INTRODUCTION

The potential of thin films prepared by pulsed laser deposition (PLD) for electrochemical applications has only been recognized recently, but the number of studies is increasing steadily. There are also still new directions in electrochemistry to be explored, where PLD films have not yet been applied, but with a large future potential. Some examples are discussed in the context of possible future directions and in the conclusions of this chapter. The reason for the late recognition of PLD films for electrochemical studies is probably related to the fact that many electrochemical studies are associated with wet chemistry, that is, liquid electrolytes. This environment is probably still quite exotic for many groups that work in the typical vacuum environment of PLD. Another reason is the fact that electrochemistry is a fairly applied research field, where many of the materials are mass products and therefore not really a target for PLD films.

The recent importance of renewable energy sources has sparked research in electrochemistry on very fundamental and applied levels. The most prominent applications are rechargeable batteries and fuel cells, and many car manufacturers have already built a fuel cell car because fuel cell cars are considered to be one of the most promising options for future sustainable mobility [Junker et al., 2001; Folkesson et al., 2003; Linssen et al., 2003; Shukla et al., 2003]. Both types of electrochemical power storage/generation have been, in principle, known for a long time (a short history is given below), but fuel cell technology is not yet cost-competitive. One of the most important drawbacks are the materials, which are either very expensive noble metals (e.g., Pt as catalysts in polymer electrolyte membrane fuel cells) or are lacking in performance and/or stability. It is therefore one of the main future tasks to identify and develop new materials that will fulfill the necessary requirements. PLD has the potential to be a very useful tool for this research and can play an important role in two different ways: that is, for material development and as a method to produce model systems for parametric studies.

The first approach utilizes one of the major strengths of PLD, that is, the synthesis of materials that cannot be obtained by other methods (metastable phases [Gupta et al., 1994; Lowndes et al., 1996; Krebs 1997; Gorbunov et al., 2002; Levin et al., 2003]), or in combination with the recent development of combinatorial approaches [Koida et al., 2002; Lippmaa et al., 2002; Takahashi et al., 2002; Aronova et al., 2003; Ohkubo et al., 2003] to PLD as a fast screening method for a systematic variation of material compositions. Both approaches can easily be utilized to test and develop new more efficient catalysts, for example, the systematic variation of an $A_xA'_{1-x}BO_3$ perovskite where x

Pulsed Laser Deposition of Thin Films: Applications-Led Growth of Functional Materials
Edited by Robert Eason

is varied in discrete steps. The other important role of PLD is the possibility of preparing model systems, which is, of course, closely related to the above described material developments.

Most electrochemical systems have one major feature in common: They are applied as electrodes, electrolytes, and electrocatalyst in electrodes. Electrodes, for example, are normally complex systems that often contain an electrocatalyst, a catalyst support material, and many other components. One of the most common materials in electrodes is carbon, which has the necessary conductivity, but is also active for many catalytic reactions, for example, oxygen reduction and evolution (see Figs. 22.12 and 22.13). The other important parameter for electrochemical systems is the stability of its components, for example, the catalyst in an environment that is chemically very reactive, that is in alkaline or acidic solution with an applied potential. The two important parameters for the electrocatalyst, that is, the stability and reactivity are therefore nearly impossible to study with real electrodes that contain many elements.

The activity of the electrode, for example, cannot be directly assigned to the catalyst but is very often a superposition of all components, including the active carbon, and parameters such as the active area of the catalyst, which is nearly impossible to determine with a porous multicomponent electrode, where the catalyst is on a support material. The stability of the catalyst can also not really be tested in these electrodes because the failure of any given component or of the mechanical stability of the electrode determines this process. PLD films are, therefore, the ideal candidates to test the activity and stability of various electrocatalysts, electrodes, and electrolytes because it is possible to prepare dense films with well-known surface areas, without any support material on an electrochemically inactive substrate, such as MgO. The well-defined surface area of PLD films allows the direct comparison of the catalytic activity for different materials, or even for different crystallographic properties, such as amorphous versus single-crystalline materials.

All of these special features of PLD films and the PLD technique with all of its variations are, therefore, a perfect match for electrochemical studies. In the following paragraphs a short overview of the history and function of the most important electrochemical systems is given to provide the necessary background to understand the aim and application of PLD films in electrochemistry. The figures in the description part show also the structure of the different electrochemical devices and can be used to identify the functionality of the materials that are prepared by PLD.

22.1.1 Description and History of the Most Important Electrochemical Systems

22.1.1.1 Batteries

History During the last decade batteries have become one of the most important objects in our everyday lives because they deliver power to a plethora of often portable devices, such as clocks, detectors, remote controls, and computers. Batteries have come a long way since the first "battery," which was dated around 250 B.C. (Baghdad, Iraq), but there are still many possibilities for further improvements. The first batteries were used in simple operations to electroplate objects with a thin layer of metal while the next generation of batteries was invented as a matter of curiosity, in the anatomical studies of frogs. Luigi Galvani observed that the muscles in a frog's leg would contract when jolted with a static electrical spark delivered from a Leyden jar. He additionally noticed that the frog's leg also reacted to two different metals being applied to the muscle, deducing that the muscle was producing electricity. Based on the results of Galvani, Alessandro Volta developed in 1798 a device made of alternating pieces of electrolyte (sodium chloride salt) soaked disks, zinc, and copper disks stacked in a column with a wire connected to a copper plate on the top, and a wire connected to a zinc plate on the bottom. This more or less started modern electrochemistry and the unit of electrical potential was named "volt," to honor one of the first inventors. In the nineteenth century various incremental improvements and discoveries for batteries were implemented. The next important invention came from Gaston Plantè, who developed the lead–acid cell in 1859. This was the first successful storage cell, or rechargeable battery. The following major development was the wet cell invented by Leclanché in

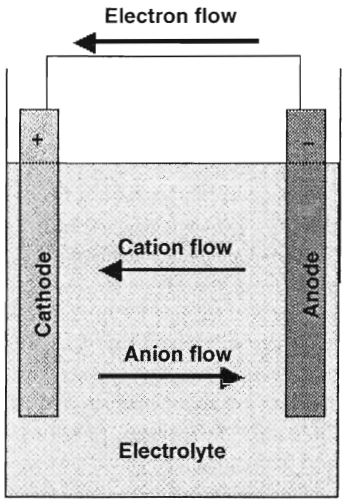

Figure 22.1 Schematic of a battery, indicating the charge flow and charge carriers inside and outside of the battery. Electrons start to flow from the anode to the cathode when the external circuit is closed. This current flow is compensated in the battery by a flow of ions between the electrodes.

1866. Further improvements of battery technology were limited by the liquid electrolyte, however. The dry cell, which is very similar to today's carbon–zinc batteries, was developed in 1888 by Carl Gassner and first sold in 1896. The twentieth century was characterized by the development and optimization of new materials, which resulted in 1959 in the first commercially available alkaline battery. In the 1960s the first silver oxide system and the first nickel cadmium rechargeable batteries became available, followed by rechargeable Li ion batteries in 1962 and Ni metal hydride batteries in the late 1960s [McNicol and Rand, 1984].

Description A battery, which is actually an electric cell, is a device that produces electricity from a chemical reaction. Strictly speaking, a battery consists of two or more cells connected in series or parallel, but the term can also be generally used for a single cell. A cell consists of a negative electrode, an electrolyte, which conducts ions, a separator, which is also an ion conductor, and a positive electrode. The electrolyte may be aqueous or nonaqueous, as a liquid, paste, or also in solid form. The negative electrode supplies a current of electrons that flow through the load and are accepted by the positive electrode (Fig. 22.1) when the cell is connected to an external load or device to be powered. The reaction stops when the external load is removed. Two types of batteries exist, depending on how the stored energy in the cell is produced. A primary battery can convert its chemicals into electricity only once and is then discarded (one way battery). A secondary battery has electrodes that can be reconstituted by passing electricity back through them. This type of battery is called a storage or rechargeable battery and can be reused many times.

The voltage of a battery is a characteristic of the cell design and the chemical reactions taking place inside. Nevertheless, the voltage changes with temperature, age of the cell, and load. A single cell can produce anything from a small fraction of a volt to more than 3 V, depending on the type of battery. In this context we would like to remind the reader about some fundamental definitions about batteries, which will be used later in this chapter. The capacity of a battery is the amount of electricity or electric charge that can be delivered during discharge at constant current until the final discharge voltage is reached. The standard unit to measure the capacity is the coulomb (C). The battery capacity is generally expressed by ampere-hours (Ah) or milliampere-hours (mAh). The total energy of a battery is expressed by watt-hours (Wh) (capacity $\times$ voltage), while the storage density of a battery is the ratio of capacity to its weight [McNicol and Rand, 1984].

Selected Battery Types

ZN–AIR BATTERIES The first Zn–air cell employing an alkaline electrolyte was patented in 1894 and consisted of a central Zn electrode, a porous separator, an inner fine particulate carbon layer, an outer particulate carbon layer, and a perforated Ni current collector. Cells of this type have capacities in the range from 300 to 3000 Ah, with a specific power of less than 1 W/kg. Recently, the interest in this type of battery was renewed, as many technical problems could be solved and batteries of this type became commercially available. The Zn–air battery is the battery that offers the highest storage density, which is due to the fact that one of the components in the reaction comes from outside of the battery, that is, atmospheric oxygen from the air as cathode reactant. A Zn–air battery is also characterized by a long stable life when sealed, for example, a loss of only $\approx 2\%$ of its capacity is experienced after one year of storage (for a cell voltage of 1.65 V).

The recent design of a Zn–air battery consists of two electrodes, that is, Zn paste and a bifunctional oxygen electrode with an integrated electrocatalyst for reduction and evolution of oxygen. The reactions during discharge and charge, involving a bifunctional catalyst, can be described as follows:

Discharge	Charge
Zn Electrode	
$Zn + 4\ OH^- \Leftrightarrow Zn(OH)_4^{-2} + 2e^-$	$Zn(OH)_4^{-2} \Leftrightarrow ZnO + H_2O + 2OH^-$
Bifunctional Air Electrode	
$\frac{1}{2}O_2 + H_2O + 2e^- \Leftrightarrow 2OH^-$	$2OH^- \Leftrightarrow \frac{1}{2}O_2 + H_2O + 2e^-$

The reversible oxygen electrode potential is 0.401 V in an alkaline solution. One characteristic of this electrode is the large overpotential in the range of 0.2–0.4 V for both O_2 reactions [McNicol and Rand, 1984].

LI ION BATTERIES Lithium is an excellent material for a storage device, as electrons are very easily delivered and the element is of intrinsically low weight. One of the major problems of Li-based systems is the reactivity toward moisture, resulting in the requirement of a moisture-free environment for the production of Li ion batteries. Li ion batteries can be divided into nonrechargeable and rechargeable systems. The most common material in a nonrechargeable battery is the lithium–manganese spinel ($LiMn_2O_4$), where Li is used as the anode, the spinel as the cathode, with a carbonate electrolyte. The cell voltage of this type of battery is about 3 V. The latest generation of nonrechargeable batteries uses a polymer electrolyte and are intended for lightweight portable equipment. Rechargeable lithium ion batteries are important for space and portable power applications. The development of rechargeable batteries using lithium started in 1912, but only became commercially available in 1991 (by Sony). The rechargeable Li ion batteries were an instant success due to their light weight and long shelf life. Current systems use a carbon anode that inserts lithium ions from the cathode through the electrolyte (Fig. 22.2). The latest step in lithium ion battery development (1996) was the replacement of the liquid electrolyte with a polymer gel electrolyte, resulting in a high product safety [McNicol and Rand, 1984].

22.1.1.2 Fuel Cells

History The first fuel cell was developed by Sir William Robert Grove in 1839, who mixed hydrogen and oxygen in the presence of an electrolyte and produced electricity and water. The invention, which later became known as a fuel cell, did not produce enough electricity to be useful,

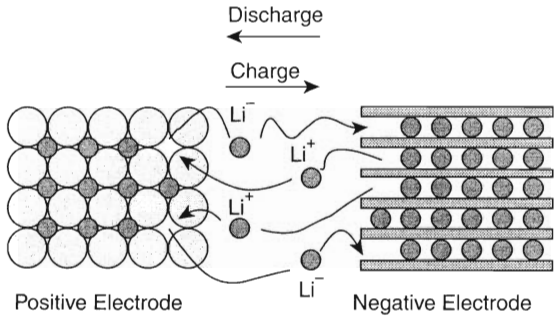

Figure 22.2 Schematic of a lithium ion battery, with the positive and negative electrode, which are separated by an electrolyte. If the electric circuit is closed, Li^+ ions are intercalated from the negative electrode through the electrolyte into the positive anode. This process can be inverted by applying a reverse outer current.

however. In 1889, the term "fuel cell" was probably first coined by Mond and Langer, who attempted to build a working fuel cell using air and industrial coal gas, while other sources attribute the term to W. Jaques. Jaques was also the first researcher to use phosphoric acid in the electrolyte bath. Fuel cell research in Germany paved the way in the 1920s to the development of today's carbonate cycle and solid oxide fuel cells. Important developments in 1959 by F. Bacon resulted in a design that was applied for a 5-kw fuel cell that could power a welding machine. In October 1959, Harry Karl Ihrig, demonstrated a 20-hp tractor that was the first vehicle ever powered by a fuel cell. The first bus powered by a fuel cell was completed in 1993, and several fuel cell cars are now being built in Europe, Japan, and in the United States. Daimler Benz and Toyota launched prototype fuel-cell-powered cars in 1997, while Daimler Chrysler unveiled the liquid hydrogen vehicle NECAR 4, in April 1999, with a top speed of 90 mph and a 280-mile tank capacity. Another fuel cell car has been developed by the Volkswagen group and a group of researchers based in Switzerland (PSI, ETH, Montena SA, FEV Motorentechnik GmbH, EMPA) and was tested in January 2002.

Description Fuel cells are based on reverse electrolysis and resemble batteries because their direct current (DC) electrical output is due to an electrochemical process: unlike batteries, they will continue to deliver energy as long as fuel is supplied. Fuel cells consist of two electrodes, which are separated by an electrolyte. An oxidant is fed to the cathode to supply oxygen, while hydrogen is supplied at the anode side (Fig. 22.3). An individual fuel cell generates from 0.6 to 0.8 V DC, with a conversion efficiency of up to 50%. High power outputs can be generated by designing large numbers of cells that are connected in series. There are various types of fuel cells that operate at different temperatures (i.e., from below 100°C to above 1000°C). In general, two classes of fuel cells are known, termed alkaline and acidic. There is just one type of alkaline fuel cell, which is also the longest known technology, which is still used in aerospace applications. There are four types of acidic fuel cells: the phosphoric acid fuel cell (PAFC), the proton exchange (or polymer) membrane (PEM)

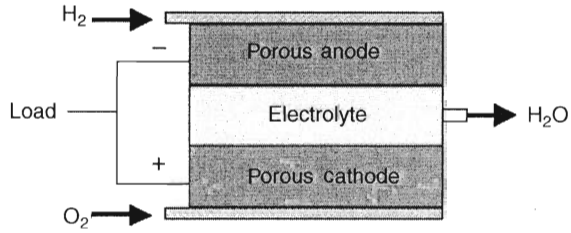

Figure 22.3 Schematic of a fuel cell, consisting of two electrodes separated by the electrolyte. An oxidant is fed to the cathode, while hydrogen is supplied to the anode.

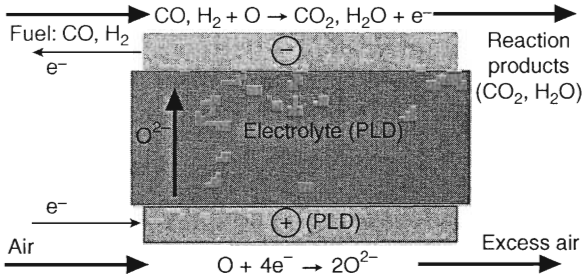

Figure 22.4 A SOFC consists of two electrodes separated by a solid electrolyte. Fuel that is delivered to the anode reacts with oxygen ions from the electrolyte and releases electrons into the external circuit. The cathode accepts electrons from the external circuit to supply the electrolyte with O^{2-} ions to maintain the overall electric charge balance.

fuel cell, the molten carbonate fuel cell (MCFC), and the solid oxide fuel cell (SOFC). The PAFC is the only acidic fuel cell that is in commercial use for stationary power generation. The PEM fuel cell was originally developed by General Electric in the late 1950s but is not yet commercially applied, except in the prototype fuel cell cars. However, there has been considerable work on the application of the PEM fuel cell in automobiles due to their low weight and low operating temperature.

Selected Types

SOLID OXIDE FUEL CELLS Solid oxide fuel cells (SOFC) are high-temperature devices and were studied by Baur and Preis in the late 1930s using zirconium, yttrium, cerium, lanthanum, and tungsten as solid oxide electrolytes. In the 1940s, O.K. Davtyan added monazite sand to a mix of sodium carbonate, tungsten trioxide, and soda glass to increase the conductivity and mechanical strength, but various undesired chemical reactions occurred. The SOFC still reveals problems due to the high internal resistance, melting, and semiconductivity, which can result in a short circuit. Westinghouse experimented with a cell using zirconium oxide and calcium oxide (1962), but only recently have advances in materials technology revived the interest in these SOFCs.

In SOFCs hard ceramics are applied as electrolytes instead of a liquid and the operating temperatures can reach 1000°C. The electrolyte is often a mixture of zirconium and calcium oxide that forms a crystal lattice, but other oxide combinations have also been tested. The solid electrolyte is coated on both sides with special porous electrode materials. At the higher applied temperatures, the oxygen ions (negatively charged) migrate through the crystal lattice of the electrolyte and oxidize the fuel at the anode side (Fig. 22.4). The efficiency can be as high as 60%, but the temperature requirement mainly results in stationary applications [McNicol and Rand, 1984]. Nevertheless, the solid electrolyte is still one of the key materials for future improvements.

22.2 SELECTED ELECTROCHEMICAL MATERIALS PREPARED BY PLD

22.2.1 Spinels

The spinel structure has the form of AB_2O_4, where A is a metal ion with a + 2 valence and B is a metal ion with a + 3 valence. This structure is viewed as a combination of the rock salt and zinc-blend structures. The oxygen ions are in a face-centered-cubic (fcc) close packing, where the A and B ions occupy tetrahedral and octahedral interstitial sites. The spinel structure can be divided into two types: normal and inverse spinels. In normal spinels, A^{2+} ions are on tetrahedral sites and the B^{3+} ions are on octahedral sites. In inverse spinels $B(AB)O_4$, the A^{2+} ions and half of the B^{3+} ions are on octahedral sites; the other half of the B^{3+} ions are on tetrahedral sites [Giacovazzo et al., 1999].

22.2.2 Perovskites

Perovskites are metal oxides with an empirical formula ABO_3, which crystallize into a cubic, tetragonal, orthorhombic, or rhombohedral structure. The cubic form of this material is referred to as ideal perovskite and has a unit-cell edge length of approximately 4 Å. In reality, only a few perovskite-type materials have this ideal cubic structure at room temperature, but many reach it at higher temperatures [Galasso, 1969]. In the fcc structure the *A cations* are located at the corners while the O atoms are on the faces. The *B cation* is in the center of the unit cell. A tolerance factor t was defined by Goldschmit [Chandler et al., 1993] to describe the stability limits of the perovskite structure [Eq. (22.1)]:

$$t = (R_A + R_O)/2^{1/2}(R_B + R_O) \tag{22.1}$$

where R_A, R_B, and R_O are the ionic radii. The perovskites are stable within the range of $0.75 < t < 1.0$ with t normally between 0.8 and 0.9. The stable structures below this limit are ilmenite and corundum [Wells, 1986]. The perovskite structure possesses a high degree of compositional flexibility, which allows the accommodation of a wide variety of A and B cations. Consequently, perovskites exhibit many interesting conducting and chemical properties, including catalytic activity and oxygen transport capability.

22.3 APPLICATIONS OF PLD FILMS

22.3.1 Spinels in Li Ion Batteries

Various materials have been studied over the last few years as solid electrolytes and positive/negative electrodes for lithium ion batteries. In commercial batteries the electrodes consist of a composite material (i.e., active material, binders, and conductive additives). Nevertheless, the application of thin films as model systems is becoming more and more popular due to the possibility of studying the stability and reactivity of new materials in well-defined systems. The first application of PLD as a deposition technique for Li ion battery related materials, studying mainly materials used as cathodes, was published at the end of the 1990s [Jiang et al., 1999]. Only in the last 4 years have materials for anodes and the solid electrolyte also been studied.

22.3.1.1 Cathode Materials

The most studied compound is $LiMn_2O_4$, which is used as the cathode material. One general problem for the deposition of Li-containing thin films is the fact that the films are Li deficient, but this problem can be overcome by using targets that are enriched in lithium. Inaba et al. [1999] studied the properties of a thin film of $LiMn_2O_4$ by cyclic voltammetry and scanning tunneling microscopy (STM) and observed that the surface morphology changed during potential cycling. Small spherical particles appeared on the surface after cycling. The number of particles increased while the particle size decreased with the number of cycles (shown in Fig. 22.5). The discharge

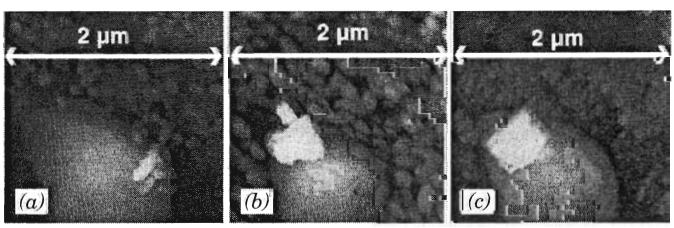

Figure 22.5 STM images ($2 \times 2\,\mu m$) of a $LiMn_2O_4$ thin film obtained after (a) 1, (b) 20, and (c) 75 cycles between 3.50 and 4.25 V in 1 *M* $LiClO_4$/propylene carbonate electrolyte solution. The sample and tip potentials were 3.5 and 3.0 V, respectively. The figure has been adapted from Inaba et al. [1999].

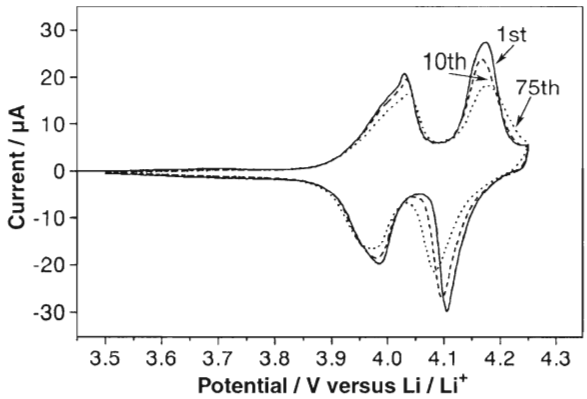

Figure 22.6 Cyclic voltammograms of a $LiMn_2O_4$ thin film deposited on Au at 873 K for 1 h. The electrolyte solution was 1 *M* $LiClO_4$/propylene carbonate electrolyte solution. The scan rate was 1 mV s^{-1}. The figure has been adapted from Inaba et al. [1999].

capacity decreased by 6% from the initial capacity in the 75th charge/discharge cycle in the range of 3.5 to 4.25 V (as derived from the cyclic voltammograms shown in Fig. 22.6).

The influence of the PLD parameters on the resulting thin films has been studied by Julien et al. [2000], who used mixtures of $LiMn_2O_4$ and Li_2O powders as targets to avoid the lithium deficiency in the resulting films. The main factor that determines the film morphology is the substrate temperature, with higher temperatures resulting in less porous films. The resulting films crystallized in a polycrystalline spinel structure and were applied in microbatteries, which presented a good specific capacity of 120 mC/cm^2 (shown in Fig. 22.7) that was attributed to the high degree of crystallinity.

One application of $LiMn_2O_4$ films has been suggested in 2001 by Singh et al. [2001] who applied the thin films in microelectromechanical systems, that is, in small-scale sensors (chip with a sensor). The deposited and applied films were highly crystalline and revealed a good kinetic behavior, cyclability, and capability for Li extraction/intercalation. Films that were deposited at higher temperatures revealed a lithium deficiency, probably due to the high vapor pressure of Li. An

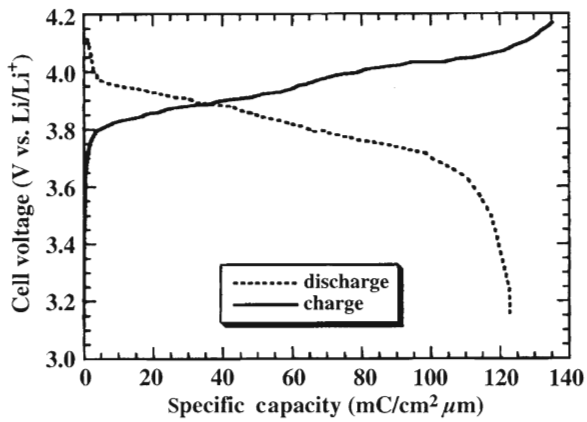

Figure 22.7 First discharge curve of a Li//$LiMn_2O_4$ microbattery using a $LiMn_2O_4$ film grown by PLD in 100 mTorr oxygen pressure onto a substrate heated to 300°C. The figure has been adapted from Julien et al. [2000].

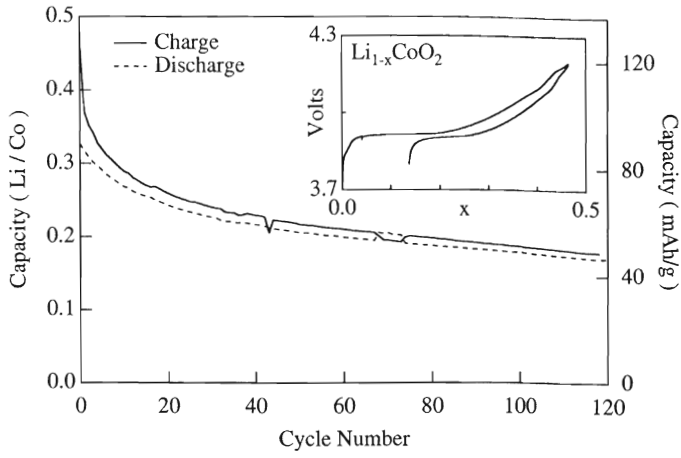

Figure 22.8 Capacity, in units of Li exchanged per Co, vs. cycle number for a 390-nm-thick $LiCoO_2$ film grown at 600°C in 200 mTorr of oxygen. The film was cycled between 3.8 and 4.2 V vs. Li at a constant current of 5 μA in a 1 *M* $LiClO_4$/propylene carbonate electrolyte solution. The inset shows the voltage vs. Li content for the first charge and discharge cycles. The figure has been adapted from Perkins et al. [1999].

ultraviolet (UV)-assisted PLD system (248 laser + UV lamp) was developed in 2002 [Singh et al., 2002] to produce films with higher crystallinity than films grown by standard PLD under the same conditions. The films with the higher crystallinity also revealed superior properties, such as a capacity loss of only 5% over a period of 1300 charge/discharge cycles.

Since 1999 [Perkins et al., 1999] other cathode materials have been studied in their pure ($LiCoO_2$) and doped ($LiCo_{1-x}Al_xO_2$) form. Perkins et al. [1999] have deposited both materials and obtained films where the Li and Co layers were oriented parallel to the substrate. The $LiCo_{1-x}Al_xO_2$ had to be deposited on a substrate with temperatures that were ≈100°C higher than in the case of $LiCoO_2$ to obtain similar grain sizes and crystallinity. For $LiCo_{1-x}Al_xO_2$ the charge/discharge curves indicates an asymmetry between Li extraction and intercalation (Fig. 22.8), which results in a capacity for the doped electrode that is three times lower than for the $LiCoO_2$ film electrode.

The influence of the film crystallinity on the Li ion diffusion has been studied by the potentiostatic intermittent titration technique (PITT) [McGraw et al., 1999]. The results indicate that the chemical diffusion coefficients are quite similar for amorphous and crystalline films, indicating that the better performance of the electrodes with higher crystallinity is not due to the Li ion diffusion. Another electrode material that has been studied is $Li_xV_2O_5$, where a completely reversible Li ion intercalation was observed. The chemical diffusion coefficient for Li ions into $LiCo_{0.5}Al_{0.5}O_2$ is at least 1–2 orders of magnitude smaller than for $LiCoO_2$. One possibility to overcome this problem is to control the amount of extracted Li, which may improve the discharge capability.

The Li ion positions in the film were analyzed as a function of the texture of the PLD films. The Li layers are oriented parallel to the substrate and perpendicular to the diffusion direction for the (003) texture in $LiCoO_2$ films, while the Li layers are separated by one cobalt and two oxygen layers along the (001) direction, which impedes the Li diffusion compared to the (003) texture [Iriyama et al., 2001]. Additional studies in the last few years [Julien et al., 2001; Julien and Gastro-Garcia, 2001] address the structure, morphology, and crystallography of Li-containing films without detailed electrochemical characterization of the films. These studies confirmed the data from older studies that indicate that it is necessary to use targets that are enriched in Li to obtain the correct stoichiometry in the resultant films. Kim et al. [2002, 2003] studied the influence of a 10-nm-thick Al_2O_3 coating on thin films of $LiCoO_2$. The coating resulted in a faster Li ion diffusion and

migration after 80 charge/discharge cycles than in films without a coating. The cycle life performance could be improved when the films were cycled only between 2.75 and 4.4 V. The reason for this improvement is the inhibition of Co dissolution during cycling. $LiCoO_2$ films loose 75% of their original capacity, while the Al_2O_3-coated films loose only 25%.

Another possible material for the cathode is V_2O_5. The first studies on thin films were performed by Julien et al. [1999] who analyzed different deposition conditions such as oxygen pressure and substrate temperature to achieve the correct film stoichiometry. Films deposited at 300°C with an oxygen background pressure of 100 mTorr present an orthorhombic polycrystalline phase where the *c*-axis is oriented perpendicular to the substrate plane. Fang et al. [2001] studied a mixture of vanadium and tungsten oxides and also the pure oxides. One innovation in this study is the application of a double layer of $WO_3(V_2O_5$ doped)/$V_2O_5(TiO_2$ doped) and not the usual mixture of the materials in the target to produce films with mixed elements. The WO_3 films degraded upon cycling, while for the V_2O_5 films the peak current density increased by up to 3% for the first three cycles followed by a constant current density over the next 1000 cycles. This long-term stability could only be obtained when the voltage sweep was limited to a *safe* range between 1.5 and 2.0 V. This limited range for the applicable voltage is due to the structure of the films where the Li ion mobility is higher between layers than across the layers. The peaks in the cyclic voltammograms for the $WO_3(V)/V_2O_5(Ti)$-layered films are due to the insertion and extraction of lithium in both layers of the double structure film (Fig. 22.9). The top layer $V_2O_5(Ti)$ is nanocrystalline and oriented in the *c* direction, which results in an improved transport of the Li ions and an increase of the cycle stability and reversibility of the $WO_3(V)$ layer.

Other dopants for V_2O_5 have been studied in the last few years to improve the electrochemical properties of this material. Huang et al. [2003] applied a composite material, such as $Li_2Ag_{0.5}V_2O_5$. The reason for choosing this material was the idea that the electrochemical properties will improve due to an expansion in the interlayer distance and an increase in the specific area of the material, which will provide better defined diffusion pathways for the Li ions. A preliminary result indicated that the PLD film could not improve the Li ion mobility during the electrochemical cycling but may still be useful as a cathode material for all-solids-state thin-film batteries. The electrochemical

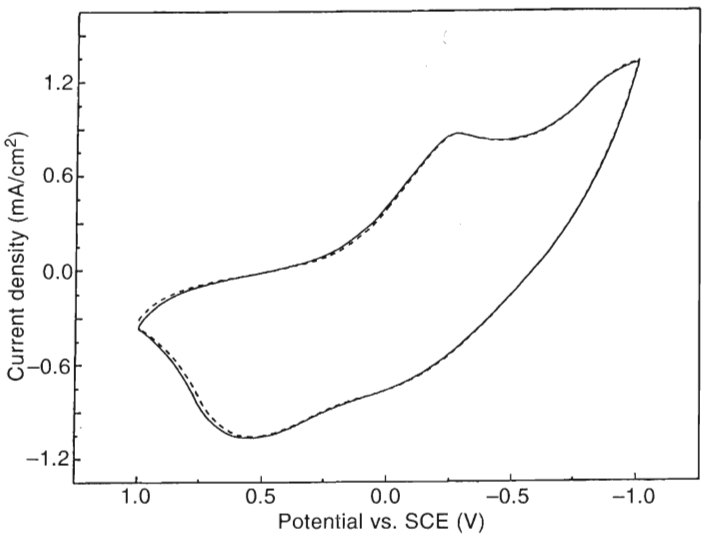

Figure 22.9 Cyclic voltammograms of WO_3 (V)/V_2O_5 (Ti) double-layer thin films deposited at 200°C on ITO with a sweep rate of 50 mV s^{-1}. The solid line represents the 4th cycle, while the dashed line represents the 1000th cycle. A saturated calomel electrode (SCE) has been used as reference electrode. The figure has been adapted from Fang et al. [2001].

properties of these films are better than for pure V_2O_5 and $Ag_{0.5}V_2O_5$ films. A capacity of 60 μAh/μm cm^2 at a current density of 7 μA/cm^2 could be reached when these films were used as cathodes. Another doped material that has been studied is NiO–V_2O_5 [Liu et al., 2003] where $(NiO)_{0.5}V_2O_5$ could be identified as the best material. The orthorhombic crystalline structure of V_2O_5 changes to an amorphous phase when the NiO content is increased. A mechanistic study concerning the extraction/insertion of Li, based on the X-ray diffraction (XRD) and X-ray photoelectron spectroscopy (XPS) results, suggests that one part of the Li ions insert and release from the vacant position within the V_2O_5 layers. The other Li ions react with the NiO, leading to the formation of metallic Ni and Li_2O. Both processes contribute to the specific capacity of the composite film, which is in the range of 340 mAh/g.

Another class of materials that has been studied are Ta_2O_5-ZnO composite films and films from the single compounds Ta_2O_5 and ZnO [NuLi et al., 2003]. Composite films with a Ta/Zn molar ratio of 2.5 exhibit the best performance in both the reversible capacity and capacity retention (up to 90% of its original capacity for up to 50 cycles). The analysis of these films revealed the formation of a crystalline orthorhombic $ZnTa_2O_6$ phase proving that the films are not just a physical mixture of ZnO and Ta_2O_5. The improvement of the Li capacity is attributed to the crystalline orthorhombic $ZnTa_2O_6$ phase.

Studies of the insertion and transport of Li in Ta_2O_5 have been made by Fu and Qin [2000a] using electrochemical methods and the isothermal transient ionic current method. The electrochemical and electrical properties of the film are strongly dependent on the film annealing parameters. Several values for diffusion constants of Li in Ta_2O_5 could be obtained in these studies, with values ranging from 2.6 to 5.2 × 10^{-15} cm^2/s. The anatase phase of TiO_2 was used as an alternative material [Fu and Qin, 2000b] and diffusion coefficients of Li ions in the range of 1.95–16 × 10^{-13} cm^2/s were obtained. The high quality of the anatase films prepared by PLD was confirmed by XRD.

22.3.1.2 Anode Materials

Only recently have the first studies been performed on anode materials, which may be an alternative to the currently used carbon materials. The first study was performed by Ding et al. [1999], utilizing SnO_2 as an electrode material. The main results indicate that there are many differences in the electrochemical properties between bulk SnO_2 and thin-film materials. The bulk material is amorphous, where the Sn(II)-O sites act as active centers for Li ion intercalation. The thin films consist mainly of nanoscale SnO crystals in an amorphous oxide matrix, where the crystalline SnO contributes to the intercalation of the Li ions. The thin films loose 56% of their capacity during the first discharge cycle compared to only 37% for the bulk material. Additionally, indications for an irreversible reaction have been detected where SnO_2 is reduced to metallic Sn during the insertion of lithium. This reaction is probably the main reason for the fast loss of capacity.

Various other materials, mainly oxides, have been studied recently as anode materials, including CeO_2 [Jiang et al., 1999], Co_3O_4 [Wang et al., 2003c], Ta_2O_5 [Fu et al., 2003], and Mg_2Si [Song et al., 2003]. The CeO_2 thin films are oxygen deficient, with a polycrystalline monoclinic structure of Ce_6O_{11}. The thin films revealed a good cycling stability with a reversible capacity of 45 mC/cm^2 (for cycling in the range of 0.1–1.5 V).

The Co_3O_4 films consist mainly of nanocrystalline particles with an average size of 50 nm. Discharge/charge cycles and cyclic voltammetry measurements reveal an irreversible reduction process during the first cycle, but also a high cycle performance following the first cycle.

The Ta_2O_5 films were amorphous and were used in rechargeable lithium ion batteries, which revealed a high reversible capacity of 400 mAh/g. This high value for the reversible capacity corresponds to more than 6 Li entering one Ta_2O_5 unit to form $Li_xTa_2O_5$. The volumetric capacity of these films is approximately four times larger than for typical graphite electrodes (5 μA/cm^2). This high capacity is due to the reaction of Ta_2O_5 with 8Li to form $2Ta_2O$ and $4Li_2O$.

The 30-nm-thick Mg_2Si films delivered a capacity that is larger than 2000 mAh/g for more than 100 cycles, suggesting the good stability of this electrode material during cycling. Thicker films (i.e., 296 and 380 nm) showed a fading rate of the capacity of about 0.5–0.6% per cycle for up to 140 cycles.

Another type of material that has been studied is $LiTi_2(PO_4)_3$, which presents a NASICON-type structure [Wang et al., 2003a]. This compound crystallizes in a rhombohedral structure with a maximum amount of 5.2 mol of Li ions that can be electrochemically intercalated per mole of $LiTi_2(PO_4)_3$. Impedance measurements indicate a quite high Li diffusion coefficient (in the range of 10^{-7}–10^{-5} cm^2/s).

22.3.1.3 Solid Electrolytes

The solid electrolyte is another very important component for the development of Li ion batteries, especially for the miniaturization of Li ion batteries as all-solid-state devices. High ion conductivity and a negligible electronic conductivity are necessary for this type of battery. Lithium phosphorus oxynitride (LiPON) as a solid electrolyte was first deposited by radio frequency (RF) magnetron sputtering, and several studies have been performed by Bates et al. [1993, 1995] who headed the development of this material and devices. Recently Zhao et al. [2002] presented the first results of amorphous LiPON films produced by PLD. An increase in the ionic conductivity could be observed when a higher concentration of nitrogen was incorporated in the films. This can be achieved by increasing the N_2 background pressure during deposition and/or by increasing the laser fluence. However, a saturation of the ionic conductivity was observed for fluences ≥ 15 J/cm^2. Unfortunately, no measurements with the PLD LiPON films were performed in batteries. These measurements will be absolutely necessary to test whether the material can be used in thin-film rechargeable lithium batteries. Another material that was also studied by Zhao and Qin [2003] is Li–V–Si–O. These thin PLD films were produced from a target that was a mixture of Li_2CO_3, V_2O_5, and SiO_2. The electrochemical window for testing this material is narrower than for LiPON and therefore less promising.

An alternative method for the fabrication of all-solid microbatteries is the so-called matrix-assisted pulsed laser evaporation (MAPLE)-DW process (see Chapter 3), where thin layers are transferred from a layered material by laser onto a substrate [Pique et al., 2001]. This method allows the fabrication of a multilayer structure, such as a battery, but without the control over crystallinity of the materials that can be achieved by PLD.

22.3.2 Perovskites in Solid Oxide Fuel Cells

Thin-film materials have significant advantages in SOFC because they allow a decrease of the operational temperature, which results in fewer problems with degradation. SOFCs consist typically of an $La_{1-x}Sr_xCoO_3$ (LSCO) layer as the cathode, an yttria-stabilized zirconia (YSZ) or $La_{1-x}Sr_xGa_{1-y}Mg_yO_3$ (LSGM) layer as electrolyte, and a metallic layer as the anode (usually nickel) (see also Fig. 22.4). The thin films must have two properties, namely high electronic and high oxygen ion conductivity. The perovskite LSCO fulfills these requirements and is therefore the most studied material. The first application of PLD as the deposition technique for cathodes and electrolytes in SOFCs was published in 1996 [Coccia et al., 1996]. The application of PLD films in electrochemical studies is not really developed and all the publications about PLD thin films in SOFCs so far only claim the importance of the material but do not present detailed results about the electrochemical properties, which are of course the most important factors to determine the possible future application of these films and materials.

22.3.2.1 Cathode Materials

The most studied compound to date is $La_{0.5}Sr_{0.5}CoO_3$. Chen et al. [1999a] have deposited this material on $LaAlO_3$ (LAO), on YSZ, and on LSGM, which itself had been deposited on $LaAlO_3$. The results indicate that on LAO and on LSGM/LAO epitaxial films were grown, while on YSZ substrates the orientation of the deposited film depends on the deposition temperature and on the oxygen background pressure. An increase of the LSCO film porosity can increase the gas transport to the reaction sites in the electrolyte (YSZ) [Chen et al., 1999b]. Epitaxial films with low resistivity (10^{-3} Ωcm) were obtained at substrate temperatures of 550°C, while at room

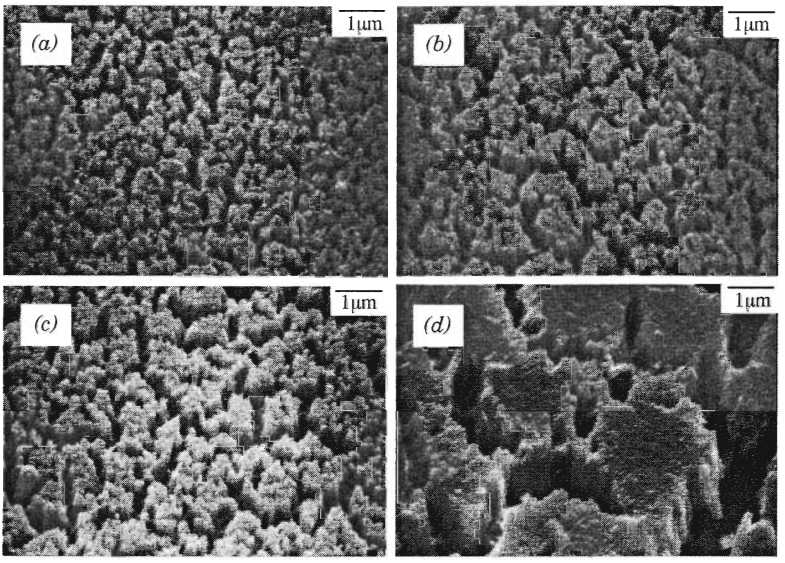

Figure 22.10 SEM images of LSCO/YSZ films annealed at different temperatures: (a) 450, (b) 550, (c) 650, and (d) 750°C. The figure has been adapted from Chen et al. [1999b].

temperature porous films were produced that reveal a high resistivity ($> 10^3\,\Omega$cm). An annealing step in air was added to reduce the resistance of the porous films, resulting in an improved resistivity of $10^{-2} - 1\,\Omega$cm. The final resistivity after annealing is a function of the annealing temperature. The size of the pores increases with increasing annealing temperature as shown in the scanning electron microscopy (SEM) image in Figure 22.10. An additional change in the structure of the film from amorphous to polycrystalline was also observed. The oxygen transport properties are another important parameter for the application of LSCO thin films in SOFCs. The effect of oxygen pressure and temperature during deposition on the crystallographic and conduction properties of the film has been analyzed [Chen et al., 1999c] in detail. (100) orientation is mainly observed for films deposited at 650°C and an oxygen background pressure of 150 mTorr, while for depositions at higher temperatures or lower oxygen pressures a preferential (110) orientation is obtained. Chen et al. [2002] studied the oxygen surface exchange coefficient of LSCO films deposited on LAO, using an electrical conductivity relaxation technique. The measured curves were fitted with a surface exchange-limited model, and the values for the epitaxial films are much smaller than those of polycrystalline films. However, a high-temperature treatment increases the surface exchange for the epitaxial films due to an increase in roughness and an increase in the number of active sites.

The composition and morphology of an LSCO target after ablation was also studied by Span et al. [1999]. Complete dissociation of the surface is achieved for fluences $> 0.7\,\text{J/cm}^2$. In this fluence range a steady-state target surface composition is obtained within 30 pulses. CoO nuclei are observed for fluences below $0.7\,\text{J/cm}^2$, which have a pronounced influence on the target composition and morphology and therefore also on the quality of the growing films.

Other materials that have been studied can be classified as variations of LSCO with a stoichiometric index of 0.5 for Ca and Sr. Coccia et al. [1996] studied $La_{0.7}Sr_{0.3}CoO_3$ and $La_{0.7}Sr_{0.3}Co_{0.2}Fe_{0.8}O_3$ as possible cathode materials, and $Ce_{0.9}Gd_{0.1}O_{1.95}$ (CGO) as possible materials for the electrolyte. The crystallographic quality of the films used as cathodes can be controlled by varying the deposition parameters, while congruent ablation of the CGO electrolyte could not be achieved. These films were enriched in Gd, by a factor of 2, compared to the target composition.

The deposition of $La_{0.8}Sr_{0.2}MnO_3$ on LAO and sapphire substrates was studied by Gnanasekar et al. [2002]. The films on LAO were highly *c*-axis oriented while the films on sapphire were highly *a*-axis oriented, but no studies on the electrochemical properties were performed or reported.

Another interesting application of $La_{1-x}Sr_xCoO_3$ is the possibility to use the films as a thermocouple, which is not directly related to SOFCs, but the thermal stability is, of course, an important property in their use in high-temperature SOFCs [Bhatt et al., 1999]. The LSCO films decompose at high temperatures, losing Co, which results in a material that consists of La_2O_3 or La_2O_3•2SrO. The highest phase stability was obtained for $La_{0.7}Sr_{0.3}CoO_3$, which again is important information for SOFCs application.

The stability of $SrFe_yCo_{1-y}O_x$ [Tunney et al., 2003] was also studied and the Fe-rich films (i.e., $y = 0.5$, 0.75, and 1.0) revealed for a thermochemical reduction treatment (2% H_2/argon gas mixture) a reversible structural change from perovskite (ABO_3) to brownmillerite ($ABO_{2.5}$).

22.3.2.2 Electrolyte Materials

The material that is mostly applied as the electrolyte in SOFCs is yttria-stabilized zirconia, but only a few studies of PLD films of this material have been performed. Hanus and Laude [1998] described the deposition of polycrystalline zirconia by PLD, where different targets were prepared that are based on zirconia and a stabilizer (i.e., Y_2O_3, MgO or CaO). The structure of the film was either tetragonal or cubic, depending on the stabilizing oxide (i.e., tetragonal for Y_2O_3 and cubic for CaO). The results also indicated that the phase structure of the deposited films was identical to that of the initial target material, independent of either the target or substrate temperature. The deposition of YSZ on NiO/YSZ was also studied [Hobein et al., 2002], and the films revealed a cubic phase with traces of the tetragonal phase for low oxygen pressures. Film deposition was also performed under various background pressures, but no improvements in gas leakage compared to the uncoated YSZ substrates was observed. One of the demands on a electrolyte is the property to prevent gas exchange between the two electrodes (O_2, H_2) but to allow the diffusion of oxygen ions. This property was evaluated by measuring the He leakage rate, which was around 2×10^{-3} mbar l/cm^2 s, compared to the requirements for fuel cells of a He leakage rate $< 1 \times 10^{-4}$ mbar l/cm^2 s. As YSZ cannot yet fulfill all requirements, other materials have also been analyzed.

Another class of material that has been used as a solid electrolyte is $La_{1-x}Sr_xGa_{1-y}Mg_yO_3$ (LSGMO). A first study of electrical conductivity was performed by Joseph et al. [2002]. Congruent film deposition of LSGMO was obtained in vacuum or by annealing of the films in air. The electrical conductivity measurements indicated that polycrystalline films are more conductive by a factor of 10 than single-crystalline films. The high quality of the LSGMO films deposited on LSCO substrates suggests a potential application of this material in SOFCs. In another study [Kanazawa et al., 2003] results were presented on the deposition of LSGMO on NiO. The as-deposited films were amorphous but crystallization was achieved by postannealing of these films. Films with a thickness of 45 μm revealed no gas leakage, which is important for SOFC applications. One theoretical study about the conduction path and disorder of the $La_{0.8}Sr_{0.2}Ga_{0.8}Mg_{0.15}Co_{0.05}O_{2.8}$ oxides at high temperatures was presented by Yashima et al. [2003]. The results suggest that the conduction path of the oxide ions is not linear between the ideal positions but reveals an arc shape starting from the sites of the $Ga_{0.8}Mg_{0.15}Co_{0.05}$ cations.

22.3.3 Perovskites in Rechargeable Zn–Air Batteries

Thin-film materials have significant advantages for Zn–air batteries because it is possible to study different catalysts without the interference of carbon, which is always used in electrodes. Most studies until now utilize the catalyst as a powder and different perovskites are used as catalysts in the electrode material [Muller et al., 1994; Hyodo et al., 1996] that also contains carbon. The main problem of identifying the best bifunctional catalyst is always the fact that in most cases a compromise between activity and stability has to be found. Until now the best performance was obtained for $La_{0.6}Ca_{0.4}CoO_3$ [Muller et al., 1994], but a recent study by Wang et al. [2003b]

presented new promising results for a combination of mixed catalysts. These catalysts are based on a mixture of $La_{0.6}Ca_{0.4}CoO_3$ with various amounts of MnO_2, CaO, or $Ni(OH)_2$. The results indicate that the catalyst composition of 15 wt% of $La_{0.6}Ca_{0.4}CoO_3$, 5 wt% of MnO_2, and 15 wt% of $Ni(OH)_2$ presents the highest discharge capacity of 1819 mAh, compared to the 1205 mAh for the normal $La_{0.6}Ca_{0.4}CoO_3$ electrode. Other new materials that have been developed for Zn–air batteries are a new type of electrolyte [Yang and Lin, 2002], that is, a composite of PEO (polyethylene oxide), PVA (polyvinyl alcohol), and a glass-fiber material. The results obtained for this material indicate that the electrolyte has an excellent mechanical strength and an electrochemical stability in the range of up to 2.4 V. An all-solid-state Zn–air battery was also assembled that revealed an electrochemical performance that was much better than those of conventional cells with polyethylene/polypropylene or cellulose separators. These recent developments are just a few examples of the ongoing developments in this field, but they suggest also new research directions that can be followed by PLD.

The first results of PLD films of a bifunctional catalyst for a Zn–air battery were shown by Striebel et al. [1995]. The rates of the oxygen reduction and evolution reactions of PLD films of $La_{0.6}Ca_{0.4}CoO_3$, $La_{0.6}Ca_{0.4}MnO_3$, and $La_{0.5}Sr_{0.5}FeO_3$ were measured with the rotating ring disk electrode technique. The order of activity was $La_{0.6}Ca_{0.4}MnO_3 > La_{0.5}Sr_{0.5}FeO_3 > La_{0.6}Ca_{0.4}CoO_3$. The $La_{0.6}Ca_{0.4}MnO_3$ film showed a slow increase in porosity with measurement time, while the $La_{0.5}Sr_{0.5}FeO_3$ was unstable. The $La_{0.6}Ca_{0.4}CoO_3$ was stable and also active for H_2O_2 reduction, and partially carbon-coated films showed higher currents for oxygen reduction than the bare films, due to oxygen reduction on the carbon. It has been determined that the oxygen reduction proceeds through a four-electron process, and that the crystallinity of the catalyst has an influence on the catalytic activity.

Thin films of $La_{0.6}Ca_{0.4}CoO_3$ have also been studied in detail by Montenegro et al. [2002]. The films revealed an epitaxial growth on (001) MgO in the (200) orientation (*c* direction of the MgO substrate) with a cubic symmetry. The epitaxial growth was also confirmed by high-resolution transmission electron microscopy (TEM) images (shown in Fig. 22.11). The activity of the PLD films for both oxygen reactions (O_2 evolution and O_2 reduction) was determined by using a three-electrode arrangement. The polarization curves in Figure 22.12 show a comparison of the activity of a PLD film, of a real electrode, and of pure carbon. The curves reveal clearly that carbon is an active material for the oxygen reactions, confirming the concept of PLD films as model systems. The

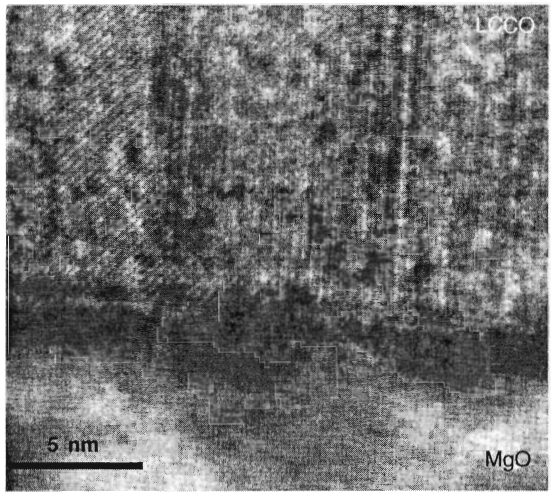

Figure 22.11 TEM image of a $La_{0.6}Ca_{0.4}CoO_3$ (LCCO) film deposited on MgO (001). The interface between the MgO and LCC is clearly visible as a darker region in the lower half of the image.

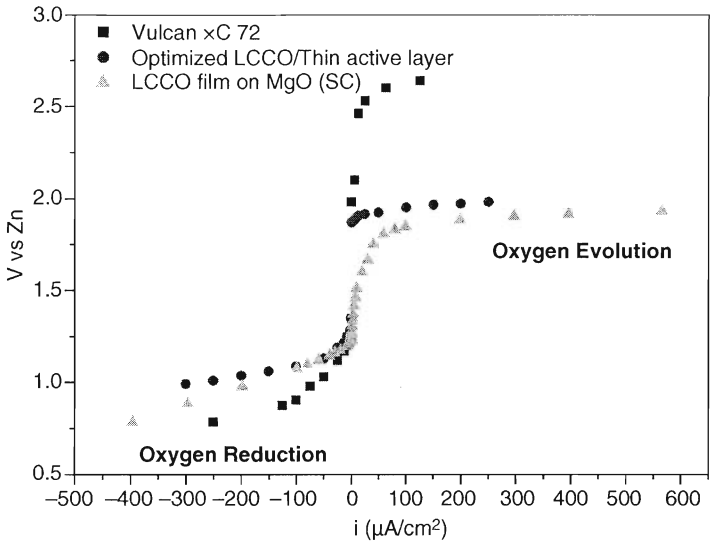

Figure 22.12 Polarization curves for carbon (Vulcan XC 72), a PLD film (LCCO film on MgO [SC (single crystalline)] and a "real" gas diffusion electrode (Optimized LCCO/thin active layer). Zn was used as a reference electrode.

polarization curves also show that PLD films present a slightly smaller overpotential than the optimized gas diffusion electrode, but also a slightly lower activity for the oxygen reduction reaction. A comparison of the activity of single-crystal and polycrystalline films (Fig. 22.13) shows a higher current density at the same voltage for a single-crystalline film on MgO than for a polycrystalline film on stainless steel. This result shows for the first time for this type of electrocatalyst that the crystallinity has a pronounced influence on the catalytic activity, that is,

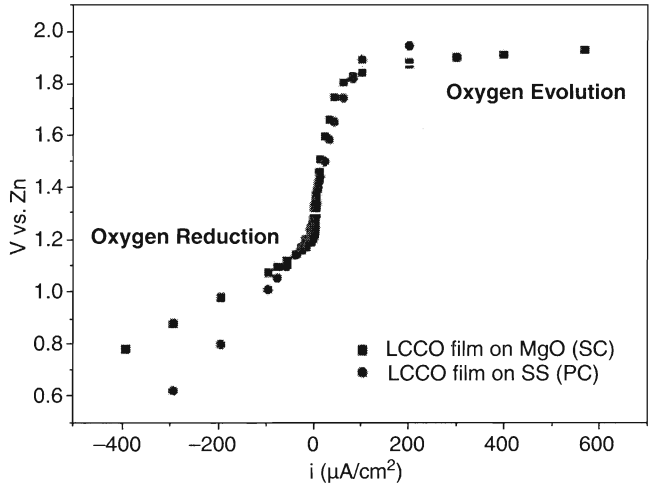

Figure 22.13 Polarization curves for a single-crystalline $La_{0.6}Ca_{0.4}CoO_3$ electrode on MgO (100) [SC (single crystalline)] and a polycrystalline LCCO electrode [PC (polycrystalline)] on stainless steel (SS). Zn was used as a reference electrode.

higher activity of the epitaxial film. This is even more remarkable when we consider that the reactions are performed in a liquid alkaline solution with an applied potential, where changes of the surface are expected.

22.4 OTHER ELECTROCHEMICALLY ACTIVE MATERIALS DEPOSITED BY PLD

22.4.1 NASICON

The growing interest in solid-state sensors has resulted in various new developments, such as gas sensors, based on advanced ionic conductors [Saito and Maruyama, 1988; Miura et al., 1994], such as NASICON (*Na* Super*I*onic *CON*ductors). NASICON is a ceramic with a complex stoichiometry ($Na_{1+x}Zr_2Si_xP_{3-x}O_{12}$ with x ranging between 0 and 3) where the specific metal can also be varied, for example, Zr or Ti. The reason for testing PLD films lies in the fact that devices usually require bulk ceramics or thick membranes, and these materials have relatively low ion conductivity and require, therefore, a high operating temperature. Thin ionic conducting films are therefore necessary for sensors to be used at room temperature as well as for microscale integration. Such films can, of course, be prepared by other methods, such as sol–gel [Schmutz et al., 1993] or sputtering [Ivanov et al., 1994], but these methods normally result in porous films with a possible deficiency of P and Na. PLD is a potential candidate for the preparation of thin NASICON films because one of its inherent capabilities is to achieve congruent film deposition of materials with complex stoichiometries.

The first NASICON PLD film was deposited on SiO_2/Si substrates. X-ray photoelectron measurements were performed to prove that congruent transfer from the target had been achieved. The films revealed lower roughness when deposited at lower fluences; at higher fluences rough surfaces with columnar structures were obtained. Electrical measurements revealed good ionic conductivity with an activation energy for ion transport of 0.5 eV, which is in good agreement with the value of 0.46 eV obtained for NASICON pellets [Izquierdo et al., 1996]. Thin NASICON films on Si with varying compositions, such as $NaM_2(PO_4)_3$ with M = Zr or Ti, have been studied with various techniques [Morcrette et al., 1997). Titanium-based compositions yield smooth films that can only be crystallized by postdeposition techniques, while zirconium-based films crystallize during the deposition process but exhibit a rough morphology. Mixtures of Ti and Zr in the target lead to smooth partly crystallized films. The composition of the films was analyzed by Rutherford backscattering spectrometry (RBS), and a systematic deviation of the Zr-based film composition from the target (Zr enrichment with P depletion) was found. In the case of Ti-based NASICON films a loss of phosphorus was also detected, but this loss could be minimized by increasing the oxygen background pressure during deposition, and nearly congruent transfer was achieved for a pressure of 0.5 mbar. No tests of the ion conductivity were performed for these films.

Another application of NASICON films is in electrolysis and bipolar membrane electrodialysis cells for splitting salts into their acid and base components. Thick NASICON films ($> 25\,\mu m$) [Joshi et al., 1994] and composite membranes [Yelon et al., 1999] have been used as sodium selective membranes for sodium sulfate splitting, which is used for the regeneration of chemicals. The composite membrane combines the advantages of polymeric membranes (thin and flexible but with low selectivity and lifetime) and ceramic membranes (high selectivity, long lifetime, but rather thick). One way to produce these composite membranes is the deposition of the ceramic NASICON onto a polymeric membrane (e.g., Raipore). PLD has been used to deposit NASICON films on Raipore and resistivities between $3 \times 10^3\ \Omega cm$ and $5 \times 10^4\ \Omega cm$ have been obtained (depending on deposition conditions), which are slightly larger than the best values for crystalline and amorphous bulk NASICON. Almost no Na depletion on the membranes was detected by elastic recoil detection analysis (ERDA), if the polymeric membrane was soaked prior to deposition in Na_2SO_4. The performance of the membranes was evaluated by measuring the current efficiency for the production of NaOH from Na_2SO_4 using electrolysis. The composite membrane with the

PLD-deposited NASICON film showed a 23% improvement compared to the polymeric Raipore membrane [Izquierdo et al., 1997; Meunier et al., 1998]. Further tests of the composite membranes with the NASICON film grown by PLD revealed a remarkable resistance of the membrane to fouling by iron compared to the polymer membrane. The ceramic layer did not affect the water transport properties of the base polymeric membrane or its selectivity to potassium and sodium. The lower electrical resistance of the thin composite membrane compared to thick freestanding ceramic membranes resulted in lower energy requirements for the production of NaOH and H_2SO_4 from Na_2SO_4 [Girard et al., 1999]. A comparison between composite membranes where the ceramic NASICON film was deposited by PLD or magnetron sputtering revealed that there was nearly no difference between the composite membranes fabricated by the two deposition techniques, although the PLD-deposited films appeared to degrade less (physically and chemically) during electrolysis [Cormier et al., 2002].

22.4.2 Noble Metals in Polymer Electrolyte Membrane Fuel Cells

It has been known for years that the cost of polymer electrolyte membrane fuel cells (PEMFCs) must be lowered to realize a commercially viable product. The amount of the platinum catalyst must be reduced to the lowest possible levels, and a first step has been taken by applying supported platinum on carbon black. This has already reduced the amount of Pt loading from several mg/cm^2 to about 0.4 mg/cm^2, but further reductions are still necessary. One possibility to lower the Pt loading is to use a deposition technique that allows very precise control of the amount of deposited Pt. One very promising techniques is PLD where deposition rates of approximately 6.75×10^{-7} mg Pt/cm^2/pulse [Cunningham et al., 2003] can be achieved. The Pt was deposited onto commercially available (E-TEK) uncatalyzed gas diffusion electrodes and compared to standard electrodes with a Pt loading of 0.4 mg/cm^2. The PLD-loaded electrodes that contained as little as 0.017 mg Pt/cm^2 performed as well as the standard electrodes that contain about 25 times more Pt (shown in Fig. 22.14). XRD and SEM analysis of the PLD-deposited Pt suggests that the deposits are made of 13-nm-diameter crystalline Pt that is evenly dispersed on the electrode. This study clearly proves that the Pt loading in PEMFCs can be further reduced, which is one important step in the direction of commercially available PEMFCs.

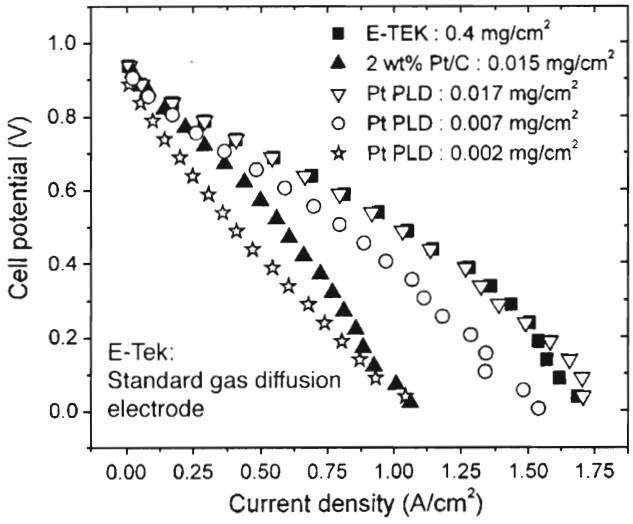

Figure 22.14 Fuel cell tests using Pt PLD electrodes on the anode side. Polarization curves for the standard E-TEK (0.4 mg Pt/cm^2) and for 2 wt % Pt/C are shown for comparison. The cathode is always a standard E-TEK (0.4 mg Pt/cm^2). The figure has been adapted from Cunningham et al. [2003].

22.5 FUTURE DIRECTIONS: DIAMOND-LIKE CARBON

One class of materials that has been prepared by PLD but has not been tested in an electrochemical context is diamond-like carbon (DLC). The properties of amorphous carbon films, both hydrogenated (a-C:H) and pure (a-C), resemble those of polycrystalline diamond films: they are very hard, electrically insulating, chemically inert, very good heat conductors, light weight, with large bandgaps, and a high index of refraction. Therefore, a-C and a-C:H are commonly referred to as diamond-like carbon, with its unique mixture of sp^2 and sp^3 carbon bonding. The combination of ceramic-like (high-hardness) and polymeric-like (high ratio of hardness to elastic modulus and low surface energy) properties suggests tribological applications that have recently been reviewed for PLD films by Voevodin et al. [1997], and see Chapter 23. Applications of DLC in electrochemical applications can be as corrosion protection of materials such as superconductors, ferroelectrics [Aoqui et al., 1998], and magnetic materials [Tomcik et al., 2000]. An additional field of application is possible for conductive doped DLC (doped with transition metals, nitrogen, boron, etc.). The resistivities of the doped DLC can be lower by 18 orders of magnitude (10^{-4} Ωcm) than for undoped films (10^{14}–10^{15} Ωcm) [Bozhko et al., 1995]. The low resistivity of these films allows an application as electrodes for electrochemical analysis [Kautek et al., 1996; Zeng et al., 2003]. Special features of a conductive-DLC electrode are a low double-layer capacitance, a large electrochemical potential window, and a relatively high electrochemical activity toward reduction of various species, such as ferricyanide. In addition, these electrodes may exhibit catalytic activity as well as durability to high anodic potential, and a high signal for the trace analysis of, for example, Pb^{2+}. These characteristics demonstrate a great potential of DLC films as a novel electrode material for electrochemical analysis [Pleskov et al., 2002; Ting and Lee 2002; Zeng et al., 2002]. Both types of application (protective coating and as an electrode) have not yet been tested for DLC films prepared by PLD. For a full discussion of PLD-deposited DLC, see Chapter 15.

22.6 CONCLUSION

The application of PLD films for electrochemical applications is still a young and growing field. Most advanced electrochemical studies to date are directed at Li ion batteries, where all components, that is, cathode, anode, and solid electrolyte, have been prepared by PLD, which were used to assemble complete all-solid-state Li ion batteries that have, of course, a great potential in the future field of miniaturization. PLD has clearly shown its potential to explore new materials, for example, the $ZnTa_2O_6$ phase, or the layered structures that cannot be prepared easily by other methods. An improved understanding of the functionality of different materials and of the processes, such as the Li intercalation (Li diffusion coefficients), is an important aspect of Li ion battery research. Further improvements of Li ion battery technology are closely related to the development of improved material research, and PLD is a very promising technique for these studies. Another already quite advanced research field of NASICON films as electromembranes has already resulted in a patent about the application of PLD for membrane synthesis.

The utilization of PLD films in other electrochemical fields still requires detailed electrochemical characterization of the thin films, and this is especially true for films related to SOFCs, where many studies stop with the physical/structural characterization of the films. A better correlation between film growth and electrochemical application is imminent in this new exciting field. The design and characterization of the electrocatalysts in Zn–air batteries and polymer electrolyte fuel cells have already proven that PLD has an important future in electrochemistry. The application of PLD films for a fundamental understanding of the catalytic processes in Zn–air batteries has already provided detailed insight and yielded new results. It could be determined that the oxygen reduction proceeds through a four-electron process, and that the crystallinity of the catalyst has an influence on the catalytic activity. Future studies will also help to identify better catalysts. Another strength of PLD, namely the precise control over the deposited material, could be used to determine the minimum

amount of Pt necessary as a catalyst in PEM fuel cells, which is of great importance for cost reduction. The high cost of PEM fuel cells is one of the major drawbacks, and the Pt concentration is one important contribution.

Other future directions of PLD lie in the preparation of miniaturized all-solid-state devices, such as Li ion batteries, Zn–air batteries, SOFCs, and even supercapacitors (where RuO_2 films could be used as electrodes).

Acknowledgments

Financial support of the Paul Scherrer Institut is gratefully acknowledged.

REFERENCES

Aoqui, S., Ebihara, K., and Yamagata, Y. (1998), *Carbon*, **36**, 591–594.

Aronova, M. A., Chang, K. S., Takeuchi, I., Jabs, H., Westerheim, D., Gonzalez-Martin, A., Kim, J., and Lewis, B. (2003), *Appl. Phys. Lett.* **83**, 1255–1257.

Bates, J. B., Dudney, N. J., Gruzalski, G. R., Zuhr, R. A., Choudhury, A., Luck, C. F., and Robertson, J. D. (1993), *J. Power Sources* **43**, 103–110.

Bates, J. B., Dudney, N. J., Lubben, D. C., Gruzalski, G. R., Kwak, B. S., Yu, X. H., and Zuhr, R. A., (1995), *J. Power Sources* **54**, 58–62.

Bhatt, H. D., Vedula, R., Desu, S. B., and Fralick, G. C. (1999), *Thin Solid Films* **350**, 249–257.

Bozhko, A., Ivanov, A., Berrettoni, M., Chudinov, S., Stizza, S., Dorfman, V., and Pypkin, B. (1995), *Diamond Relat. Mater.* **4**, 488–491.

Chandler, C. D., Roger, C., and Hampdensmith, M. J. (1993), *Chem. Rev.* **93**, 1205–1241.

Chen, X., Wu, N. J., and Ignatiev, A. (1999a), *J. Eur. Ceram. Soc.* **19**, 819–822.

Chen, X., Wu, N. J., Ritums, D. L., and Ignatiev, A. (1999b), *Thin Solid Films* **342**, 61–66.

Chen, X., Wu, N. J., Ignatiev, A., Zhang, Z. H., and Chu, W. K. (1999c), *Thin Solid Films* **350**, 130–137.

Chen, X., Wang, S., Yang, Y. L., Smith, L., Wu, N. J., Kim, B. I., Perry, S. S., Jacobson, A. J., and Ignatiev, A. (2002), *Solid State Ionics* **146**, 405–413.

Coccia, L. G., Tyrrell, G. C., Kilner, J. A., Waller, D., Chater, R. J., and Boyd, I. W. (1996), *Appl. Surf. Sci.* **96-8**, 795–801.

Cormier, L. M., Ma, F., Bah, S. T., Guetre, S., Meunier, M., Paleologou, M., and Yelon, A. (2002), *J. Electrochem. Soc.* **149**, D21–D26.

Cunningham, N., Irissou, E., Lefevre, M., Denis, M. C., Guay, D., and Dodelet, J. P. (2003), *Electrochem. Solid-State Lett.* **6**, A125–A128.

Ding, F., Fu, Z. W., Zhou, M. F., and Qin, Q. Z. (1999), *J. Electrochem. Soc.* **146**, 3554–3559.

Fang, G. J., Yao, K. L., and Liu, Z. L. (2001), *Thin Solid Films* **394**, 64–71.

Folkesson, A., Andersson, C., Alvfors, P., Alakula, M., and Overgaard, L. (2003), *J. Power Sources* **118**, 349–357.

Fu, Z. W., and Qin, Q. Z. (2000a), *J. Electrochem. Soc.* **147**, 4610–4614.

Fu, Z. W., and Qin, Q. Z. (2000b), *J. Phys. Chem. B* **104**, 5505–5510.

Fu, Z. W., Huang, F., Chu, Y. Q., Zhang, Y., and Qin, Q. Z. (2003), *J. Electrochem. Soc.* **150**, A776–A782.

Galasso, F. S. (1969), *Structure: Properties and Preparation of Perovskite-type Compounds*, Pergamon, London.

Giacovazzo, H., Monaco, H. L., Artiolio, G., Viterbo, D., Ferraris, G., Gilli, G., Zanotti, G., and Gatti, M. (1999), *Fundamentals of Crystallography*, Oxford, University Press, Oxford.

Girard, F., Izquierdo, R., Quenneville, E., Bah, S. T., Paleologou, M., Meunier, M., Ivanov, D., and Yelon, A. (1999), *J. Electrochem. Soc.* **146**, 2919–2924.

Gnanasekar, K. I., Jiang, X., Jiang, J. C., Aghasyan, M., Tiltsworth, R., Hormes, J., and Rambabu, B. (2002), *Solid State Ionics* **148**, 575–581.

Gorbunov, A., Levin, A. A., Mensch, A., Meyer, D. C., Tselev, A., Paufler, P., Pompe, W., and Eckert, D. (2002), *Appl. Surf. Sci.* **197**, 475–480.

Gupta, A., Mercey, B., Hervieu, H., and Raveau, B. (1994), *Chem. Mater.* **6**, 1011–1016.

Hanus, F., and Laude, L. D. (1998), *Appl. Surf. Sci.* **129**, 544–548.

Hobein, B., Tietz, F., Stover, D., and Kreutz, E. W. (2002), *J. Power Sources* **105**, 239–242.

Huang, F., Fu, Z. W., and Qin, Q. Z. (2003), *Electrochem. Commun.* **5**, 262–266.

Hyodo, T., Hayashi, M., Miura, N., and Yamazoe, N. (1996), *J. Electrochem. Soc.* **143**, L266–L267.

Inaba, M., Doi, T., Iriyama, Y., Abe, T., and Ogumi, Z. (1999), *J. Power Sources* **81**, 554–557.

Iriyama, Y., Inaba, M., Abe, T., and Ogumi, Z. (2001), *J. Power Sources* **94**, 175–182.

Ivanov, D., Currie, J., Bouchard, H., Lecours, A., Andrian, J., Yelon, A., and Poulin, S. (1994), *Solid State Ionics* **67**, 295–299.

Izquierdo, R., Hanus, F., Lang, T., Ivanov, D., Meunier, M., Laude, L., Currie, J. F., and Yelon, A. (1996), *Appl. Surf. Sci.* **96-8**, 855–858.

Izquierdo, R., Quenneville, E., Trigylidas, D., Girard, F., Meunier, M., Ivanov, D., Paleologou, M., and Yelon, A. (1997), *J. Electrochem. Soc.* **144**, L323–L325.

Jiang, L. Z., Zhou, M. F., Liu, X. N., and Qin, Q. Z. (1999), *Acta Phys.-Chim. Sin.* **15**, 752–756.

Joseph, M., Manoravi, P., Tabata, H., and Kawai, T. (2002), *J. Appl. Phys.* **92**, 997–1001.

Joshi, A. V., Liu, M., Bjorseth, A., and Renberg, L. (1994), U.S. Patent No. 5,290,405.

Julien, C., and Gastro-Garcia, S. (2001), *J. Power Sources* **97-8**, 290–293.

Julien, C., Haro-Poniatowski, E., Camacho-Lopez, M. A., Escobar-Alarcon, L., and Jimenez-Jarquin, J. (1999), *Mater. Sci. Eng. B.* **65**, 170–176.

Julien, C., Haro-Poniatowski, E., Camacho-Lopez, M. A., Escobar-Alarcon, L., and Jimenez-Jarquin, J. (2000), *Mater. Sci. Eng. B.* **72**, 36–46.

Julien, C., Camacho-Lopez, M. A., Escobar-Alarcon, L., and Haro-Poniatowski, E. (2001), *Mater. Chem. Phys.* **68**, 210–216.

Junker, M., Bocquet, L., Bendif, M., and Karboviac, D. (2001), *Ann. Chim.-Sci. Mater.* **26**, 117–130.

Kanazawa, S., Ito, T., Yamada, K., Ohkubo, T., Nomoto, Y., Ishihara, T., and Takita, Y. (2003), *Surf. Coat. Technol.* **169**, 508–511.

Kautek, W., Pentzien, S., Conradi, A., Kruger, J., and Brzezinka, K. W. (1996), *Appl. Surf. Sci.* **106**, 158–165.

Kim, Y. J., Kim, T. J., Shin, J. W., Park, B., and Cho, J. P. (2002), *J. Electrochem. Soc.* **149**, A1337–A1341.

Kim, Y. J., Kim, H., Kim, B., Ahn, D., Lee, J. G., Kim, T. J., Son, D., Cho, J., Kim, Y. W., and Park, B. (2003), *Chem. Mater.* **15**, 1505–1511.

Koida, T., Lippmaa, M., Fukumura, T., Itaka, K., Matsumoto, Y., Kawasaki, M., and Koinuma, H. (2002), *Phys. Rev. B* **66**, art. no.-144418.

Krebs, H. U. (1997), *Int. J. Non-Equilib. Pr.* **10**, 3–24.

Levin, A. A., Meyer, D. C., Gorbunov, A., Mensch, A., Pompe, W., and Paufler, P. (2003), *J. Alloys Compd.* **360**, 107–117.

Linssen, J., Grube, T., Hoehlein, B., and Walbeck, M. (2003), *Int. J. Hydrogen. Energy* **28**, 735–741.

Lippmaa, M., Koida, T., Minami, H., Jin, Z. W., Kawasaki, M., and Koinuma, H. (2002), *Appl. Surf. Sci.* **189**, 205–209.

Liu, H. R., Chu, Y. Q., Fu, Z. W., and Qin, Q. Z. (2003), *J. Power Sources* **124**, 163–169.

Lowndes, D. H., Geohegan, D. B., Puretzky, A. A., Norton, D. P., and Rouleau, C. M. (1996), *Science* **273**, 898–903.

McGraw, J. M., Bahn, C. S., Parilla, P. A., Perkins, J. D., Readey, D. W., and Ginley, D. S. (1999), *Electrochim. Acta* **45**, 187–196.

McNicol, B. D., and Rand, A. A. J. (Eds.) (1984), *Power Sources for Electric Vehicles*, Elsevier, Amsterdam.

Meunier, M., Izquierdo, R., Hasnaoui, L., Quenneville, E., Ivanov, D., Girard, F., Morin, F., Yelon, A., and Paleologou, M. (1998), *Appl. Surf. Sci.* **129**, 466–470.

Miura, N., Yao, S., Shimizu, Y., and Yamazoe, N. (1994), *Solid State Ionics* **70**, 572–577.

Montenegro, M. J., Dobeli, M., Lippert, T., Muller, S., Schnyder, B., Weidenkaff, A., Willmott, P. R., and Wokaun, A. (2002), *Phys. Chem. Chem. Phys.* **4**, 2799–2805.

Morcrette, M., Barboux, P., Laurent, A., and Perriere, J. (1997), *Solid State Ionics* **93**, 283–290.

Muller, S., Striebel, K., and Haas, O. (1994), *Electrochim. Acta* **39**, 1661–1668.

NuLi, Y. N., Fu, Z. W., Chu, Y. Q., and Qin, Q. Z. (2003), *Solid State Ionics* **160**, 197–207.

Ohkubo, I., Matsumoto, Y., Ueno, K., Chikyow, T., Kawasaki, M., and Koinuma, H. (2003), *J. Crystal Growth* **247**, 105–109.

Perkins, J. D., Bahn, C. S., Parilla, P. A., McGraw, J. M., Fu, M. L., Duncan, M., Yu, H., and Ginley, D. S. (1999), *J. Power Sources* **82**, 675–679.

Pique, A., Swider-Lyons, K. E., Weir, D. W., Love, C. T., and Modi, R. (2001), *Proc. SPIE* **4274**, 316.

Pleskov, Y. V., Krotova, M. D., Polyakov, V. I., Khomich, A. V., Rukovishnikov, A. I., Druz, B. L., and Zaritskiy, I. (2002), *J. Electroanal. Chem.* **519**, 60–64.

Saito, Y., and Maruyama, T. (1988), *Solid State Ionics* **28**, 1644–1647.

Schmutz, C., Basset, E., Barboux, P., and Maquet, J. (1993), *J. Mater. Chem.* **3**, 393–397.

Shukla, A. K., Jackson, C. L., and Scott, K. (2003), *Bull. Mater. Sci.* **26**, 207–214.

Singh, D., Houriet, R., Giovannini, R., Hofmann, H., Craciun, V., and Singh, R. K. (2001), *J. Power Sources* **97-8**, 826–831.

Singh, D., Kim, W. S., Craciun, V., Hofmann, H., and Singh, R. K. (2002), *Appl. Surf. Sci.* **197**, 516–521.

Song, S. W., Striebel, K. A., Reade, R. P., Roberts, G. A., and Cairns, E. J. (2003), *J. Electrochem. Soc.* **150**, A121–A127.

Span, E. A. F., Roesthuis, F. J. G., Blank, D. H. A., and Rogalla, H. (1999), *Appl. Surf. Sci.* **150**, 171–177.

Striebel, K. A., Deng, C. Z., and Cairns, E. J. (1995), *Proc. Electrochem. Soc.* **26**, 112.

Takahashi, R., Matsumoto, Y., Koinuma, H., Lippmaa, M., and Kawasaki, M. (2002), *Appl. Surf. Sci.* **197**, 532–535.

Ting, J. M., and Lee, H. (2002), *Diamond Relat. Mater.* **11**, 1119–1123.

Tomcik, B., Osipowicz, T., and Lee, J. Y. (2000), *Thin Solid Films* **360**, 173–180.

Tunney, J. J., Whitfield, P., Du, X. M., and Post, M. L. (2003), *Thin Solid Films* **426**, 221–231.

Voevodin, A. A., Donley, M. S., and Zabinski, J. S. (1997), *Surf. Coat. Technol.* **92**, 42–49.

Wang, G. X., Bradhurst, D. H., Dou, S. X., and Liu, H. K. (2003a), *J. Power Sources* **124**, 231–236.

Wang, X. Y., Sebastian, P. J., Smit, M. A., Yang, H. P., and Gamboa, S. A. (2003b), *J. Power Sources* **124**, 278–284.

Wang, Y., Fu, Z. W., and Qin, Q. Z. (2003c), *Thin Solid Films* **441**, 19–24.

Wells, A. F. (1986), *Structural Inorganic Chemistry, Clarendon*, Oxford.

Yang, C. C., and Lin, S. J. (2002), *J. Power Sources* **112**, 497–503.

Yashima, M., Nomura, K., Kageyama, H., Miyazaki, Y., Chitose, N., and Adachi, K. (2003), *Chem Phys. Lett.* **380**, 391–396.

Yelon, A., Paleologou, M., Ivanov, A., Izquierdo, R., and Meunier, M. (1999), U.S. Patent No. 5,968,326.

Zeng, A., Liu, E., Tan, S. N., Zhang, S., and Gao, J. (2002), *Electroanalysis* **14**, 1110–1115.

Zeng, A., Liu, E., Zhang, S., Tan, S. N., Hing, P., Annergren, I. F., and Gao, J. (2003), *Thin Solid Films* **426**, 258–264.

Zhao, S. L., and Qin, Q. Z. (2003), *J. Power Sources* **122**, 174–180.

Zhao, S. L., Fu, Z. W., and Qin, Q. Z. (2002), *Thin Solid Films*, **415**, 108–113.